Jordan Journal of Civil Engineering, Volume **17**, No. **1**, **2023**
DOI: https://doi.org/10.14525/JJCE.v17i1.11

Experimental and Numerical Investigations of Structural Performance of Slab Track under Hygrothermal Environment

Anxiang Song [1),2)], ***Guowen Yao*** [1),2)]*, ***Rui Zhou*** [3)], ***Xuanrui Yu*** [2)], ***Yuerui Wang*** [2)] ***and Qing Guo*** [4)]

[1)] State Key Laboratory of Mountain Bridge and Tunnel Engineering, Chongqing Jiaotong University, Chongqing 400074, China. * Corresponding Author. E-Mail: 611200080016@mails.cqjtu.edu.cn
[2)] School of Civil Engineering, Chongqing Jiaotong University, Chongqing 400074, China.
[3)] College of Civil and Transportation Engineering, Shenzhen University, Shenzhen 518060, China.
[4)] Chongqing Fengjian Expressway Co., Ltd., Chongqing 401120, China.

ABSTRACT

The coupled heat and moisture actions could easily cause deformation, cracking and corrosion problems in the slab ballastless track under operational conditions via China Railway Track System (CRTS) II. In this paper, two one-quarter-scaled models of CRTS II slab ballastless track under hygro-thermal environment were tested in a testing chamber, respectively. To study the effect of constrained conditions on the structural performance of track structure, temperature distribution, stress and displacement of two scaled models with constrained and free boundary conditions were also compared. Then, the temperature and stress field of the track structure was investigated by establishing a finite-element model. The results showed that the temperature transfer between layers has a temperature-lag effect. The positive and negative temperature gradients between the lower part of the track slab and the cement asphalt (CA) mortar layer of the constrained specimen are smaller than those of the free specimen. The longitudinal displacement of the track slab for the free specimen is significantly affected under the hygro-thermal environment and the longitudinal displacement of the concrete base and the track slab forms a displacement difference. Numerical-analysis results showed that the bottom of the concrete base is prone to produce a high-temperature core and that the temperature inside the track structure forms an agglomeration effect.

KEYWORDS: Slab track, Hygro-thermal environment, Structural performance, Scale model, Finite-element model.

INTRODUCTION

The traditional ballasted tracks are still used in high-speed railways, but with the increase in traffic speed, track breakage and deformation have increased, causing an overall decrease in track stability (Setiawan, 2022; Salama et al., 2022). Compared with ballast tracks, ballastless tracks have higher structural stability. The China Railway Track System (CRTS) II slab ballastless track-bridge structure has been widely used in high-speed railway construction and is making important contributions to the construction of modern transportation systems (Liu et al., 2015; Jiang et al., 2019; Feng et al., 2019). As presented in Fig. 1, the bridge-track structure is composed of rails, fasteners, prestressed track slabs, a cement asphalt (CA) mortar layer, a concrete base and a box girder. The track slabs are coupled in the longitudinal direction by wide narrow joints and the CA mortar layer is a flexible layer between the track slab and concrete base.

China has a vast territory and the service environment of the ballastless track is complicated, especially for the CRTS II slab track. The impacts of complex extreme environmental factors, such as temperature, humidity and corrosion, on the performance of the track structure become serious. The environmental temperature and humidity have a significant impact on the mechanical properties of the track structure with multi-layer concrete components.

Received on 28/5/2022.
Accepted for Publication on 15/9/2022.

The summer climate in southern China is hot and humid and the hygrothermal effect of the track structure is the main reason for structural damage and failure, such as structural warping deformation caused by the high-temperature environment, longitudinal buckling and interlayer gap or even void, seriously affecting its service life.

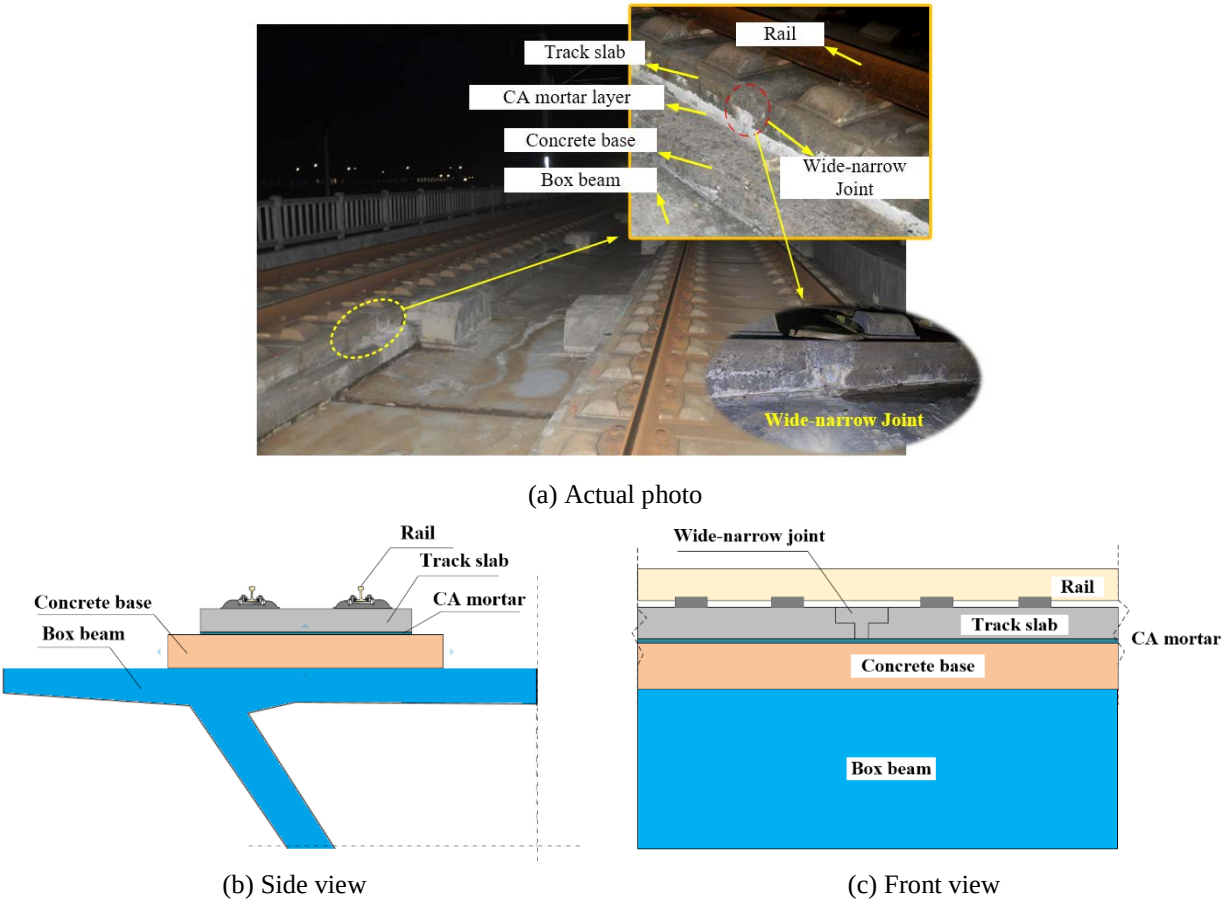

(a) Actual photo

(b) Side view

(c) Front view

Figure (1): CRTS II ballastless track-bridge

In recent years, most of the research on ballastless track mainly focused on the temperature distribution, structural stress and deformation. For example, Wang et al. (2019) analyzed the hourly climate data and determined the boundary conditions of the ballastless-track temperature field by theoretical derivation. Moreover, considering the orientation of the track structure and the geographical location, a three-dimensional calculation model of the track temperature field was established (Yang et al., 2017). A series of field tests on the temperature distribution of ballastless tracks in different seasons were conducted and the time-varying law and distribution pattern of the temperature field were studied (Dai et al., 2015a; Dai et al., 2015b; Dai et al., 2017). However, there were only a few vertical temperature-measuring points on-site, and no temperature sensors were placed on the CA mortar layer. As a result, a comprehensive understanding of the overall temperature distribution of the CRTS II ballastless track has not been established. Additionally, like other asphalt-incorporated materials, the performance of CA mortar was significantly affected by temperatures during construction and operation. Thus, based on the similarity theory, Zhao et al. (2020) and Zhao et al. (2021) established a scale model of the ballastless track and carried out a temperature test of rapid temperature rise and fall under typical high-temperature weather. The results showed that the effect of the CA mortar layer on the vertical temperature distribution of the ballastless track is significant and the temperature field has a non-linear distribution. In addition, Zhou et al. (2020a) and Zhou et al. (2020b) simulated the sunshine temperature load and cyclic temperature load and analyzed the interlayer

displacement distribution of the track structure based on the measured displacement data. Cho and Kim (2019) carried out *in-situ* experiments on continuously reinforced concrete track (CRCT) sections and presented several methods to improve CRCT performance considering the effect of temperature variation on crack width in continuously reinforced concrete track sections. Additionally, the temperature stress and deformation of ballastless tracks were explored under temperature load by combining field tests with numerical simulation and taking the most unfavorable temperature condition measured in practice as the loading basis of the numerical simulation (Yang et al., 2016; Liu et al., 2013; Wang et al., 2009; Lim et al., 2003). In summary, the existing literature mainly focuses on the temperature effect of the ballastless track. There are very few studies of the hygrothermal properties of ballastless track-bridge structures.

At present, related studies have shown that the temperature and humidity of concrete have a significant coupling effect (Chen, 2013; Min et al., 2017; Samir et al., 2010), which has an impact on the internal temperature and humidity distribution, determining the development of the volume deformation of concrete and seriously affecting the durability and service life of concrete. In general, the evolution of the mechanical properties of concrete structures in hot and humid environments has mainly focused on small-size specimens. A three-point bending fatigue test of carbon fiber-reinforced concrete beams under a hygro-thermal environment was carried out by Qin et al (2016). The results indicated that the fatigue performance of the concrete structure in a hygrothermal environment is 20% lower than that obtained in the traditional environment fatigue experiment. Li et al. (2021) carried out durability tests on polyethylene fiber concrete under temperature and humidity cycles. The results showed that the compressive strength of polyethylene-fiber concrete decreased as the number of cycles increased, but the depth of chloride ion penetration, carbonation depth and thermal conductivity increased. Černý and Drchalová (2001) explored the influence law of the water diffusion coefficient of high-performance concrete under high temperatures and pointed out that the increase of internal pressure under a high-temperature environment destroyed the micro-structure of the matrix.

However, it is difficult to carry out a performance test on the ballastless track-bridge structure under hygrothermal coupling, because the CRTS II slab ballastless track on bridges differs from ordinary concrete specimens in that it is a large, multi-layered, heterogeneous concrete structure and a testing environment for hygrothermal coupling is difficult to set up. In addition, the south China climate is characterized by high temperature and high humidity in summer and the structural performance will be complicated by the environment. Therefore, experimental structural research on the track-bridge system in a high-temperature and -humidity environment will better reflect its real mechanical issues. In summary, the existing studies have mainly focused on the performance of slab ballastless tracks under different temperature loads and there is almost no experimental research that considers both heat and humidity, especially for different boundary conditions. As a result, it is of great significance to study the hygro-thermal effects on the structural performance of ballastless tracks in a continuous high-temperature and-humidity environment to improve the service performance of ballastless tracks and ensure the safety of train operation in southern China.

This paper explores the temperature distribution, structural stress and displacement varying with time of two scale models with constrained and free boundary conditions by a test considering coupled heat and humidity parameters. Additionally, a simulation model is established to verify the test solutions and to obtain a three-dimensional temperature field for the stress field of this structure, which could realistically reveal the mechanism of the CRTS II slab track-bridge structure.

Experimental Program

Design and Fabrication of the Specimen

The CRTS II slab track–bridge structure is composed of a simply supported box girder and a ballastless track. To eliminate the boundary effects of the track–bridge structure, a 32-m prestressed simply supported concrete box-beam was selected as the prototype bridge. Due to the large size of the prototype structure, a commonly used 1:4 scaled model was used for an indoor test to accurately simulate the mechanical characteristics of the CRTS II slab track. The similarity constants between the specimen and the prototype structure were calculated by

the similarity principle, as listed in Table 1. Based on the calculation results of similar constants, the structural size of the specimen was designed, as shown in Fig. 2(a-b). In addition, scaled models of the CRTS II slab track–bridge with fixed and free constrained boundaries were established based on the similarity theory, as shown in Fig. 2(c). To achieve a fixed constrained boundary in the longitudinal direction of a scaled model, a particular steel tool was designed for the environmental testing chamber. First, two steel end plates were embedded at the ends of the scaled model and the steel tool was fixed to the pedestals of the two ends on the foundation with high-strength bolts. Eventually, the steel plate is clamped tightly between the end plate and the two hydraulic jacks installed on the steel tool. In this way, a support is created which is fixed against translation, but not against rotation. As for the free boundary conditions, the specimen is placed on supports and the ends of the specimen are free to translate.

Table 1. Similarity relationship between physical quantities of the scale model and the prototype structure

Main specifications	Prototype structure	Scale model	Similarity ratio
Size	L	L /4	1/4
Density	ρ	ρ	1
Inertial moment	I	I/256	1/256
Elastic modulus	E	E	1
Axial force	P	P/16	1/16
Vertical bending moment	M	M/64	1/64
Deformation	ε	ε	1
Stress	σ	σ	1

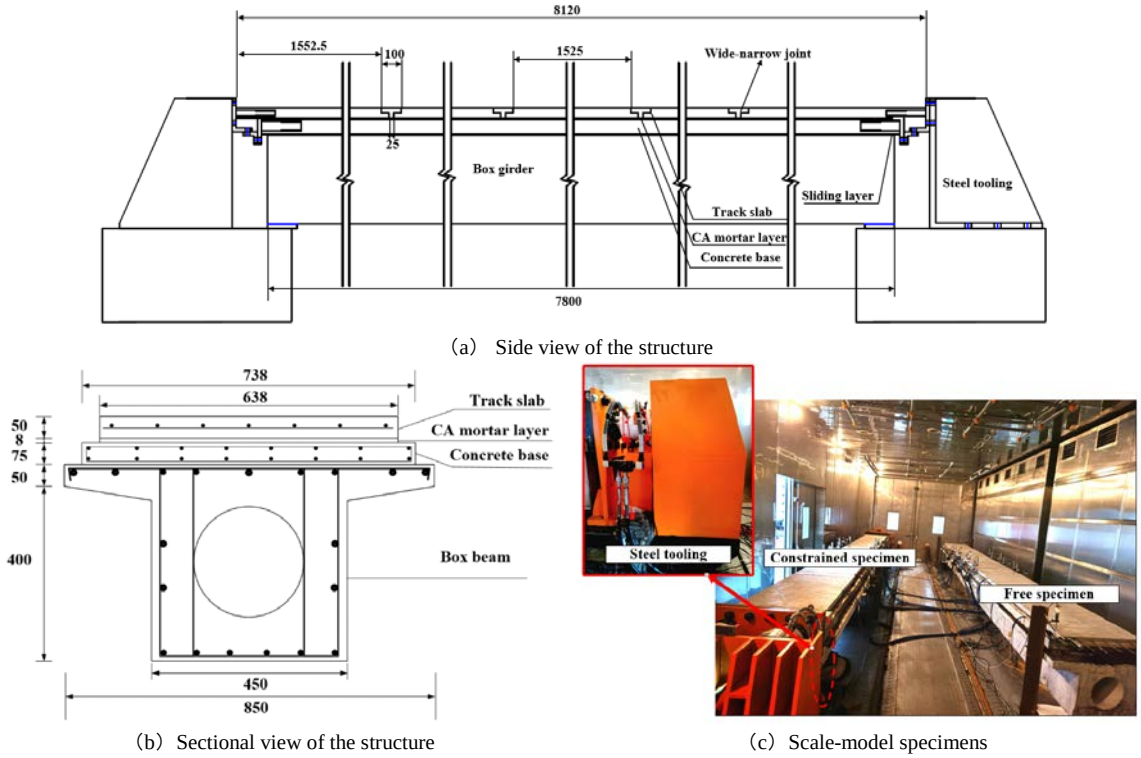

(a) Side view of the structure

(b) Sectional view of the structure

(c) Scale-model specimens

Figure (2): 1:4 scale test model of CRTSII slab ballastless track on the bridge (unit: mm)

The structural materials used in the scaled test model were consistent with the prototype structure. The track slab and the wide narrow joint concrete strength grade was C55, the concrete base strength grade was C40 and the simply supported box girder concrete strength grade was C50. The strength and modulus of elasticity of the

CA mortar layer were in accordance with the criteria for work applications. The specific material parameters are listed in Table 2.

Table 2. Material parameters of scaled-test model

Parts	Material	Density (kg/m^3)	Elastic modulus (MPa)	Poisson's ratio	Thermal expansion coefficient ($°C^{-1}$)	Thermal conductivity (W/(m·K))
Track slab	C55	2500	35500	0.2	0.00001	1.78
CA mortar layer	Asphalt	2400	8000	0.2	0.000013	1.4
Concrete base	C40	2500	32500	0.2	0.00001	1.78
Wide narrow joint	C55	2500	35500	0.2	0.00001	1.78
Simple box girder	C50	2500	34500	0.2	0.00001	1.78
Prestressed steel bars	Steel	7850	210000	0.3	0.0000118	58.2

Experimental Setup

The instrument used in this experiment is the environmental coupled loading experimental chamber from Chongqing Jiaotong University, China. The test chamber can simulate one or more climatic conditions in the large testing chamber and carry out experiments on large structures through the assembly of multiple testing chambers. The temperature of the testing chamber ranges from -40°C to 100°C and the uniformity is ±2°C. The testing-chamber humidity range is 20-98% RH and the uniformity is ±1.3% RH. Thus, the testing chamber could meet the requirements of hot and humid environment. The initial temperature of the testing chamber was 23°C. Moreover, the temperature and humidity were set according to the pre-determined set values, so as to simulate the uniform temperature field of ballastless track on the bridge under the most unfavorable conditions of high temperature and humidity. The whole process time was 24h in total. The experimental platform is shown in Fig. 3.

Measurement Devices

Temperature sensors were placed at the mid-span section and two end sections of the middle track slab, CA mortar layer and concrete base. Six layers and three rows of temperature-monitoring points were displayed in the vertical and transverse directions of two scaled models, respectively, as shown in Figure 3(a). The letters D, E and F represent the sections of the left span end, middle span and right span end for the two specimens, respectively. The strain-measuring points were also arranged at the mid-span and the two end sections of the middle track slab and concrete base. To measure the horizontal displacement of the free specimen, displacement gauges were placed at the end section of the track slab (see Fig. 4).

Figure (3): The environmental coupled loading experimental chamber

The temperature sensors were BK-318 resistance temperature sensors, where the readings were collected by a wireless temperature microcontroller unit (MCU) with an accuracy of ± 0.25℃. The strains of the track slab and the concrete base were measured by distributed fiber Bragg gratings (FBG) strain sensors, where the readings were collected by the OP-ST01 FBG demodulators with a range of ±1500 με and a precision of 0.5% FS. The displacement gauges adopt linear variable displacement transducers (LVDTs) with a range of 50 mm and an accuracy of 0.5% FS.

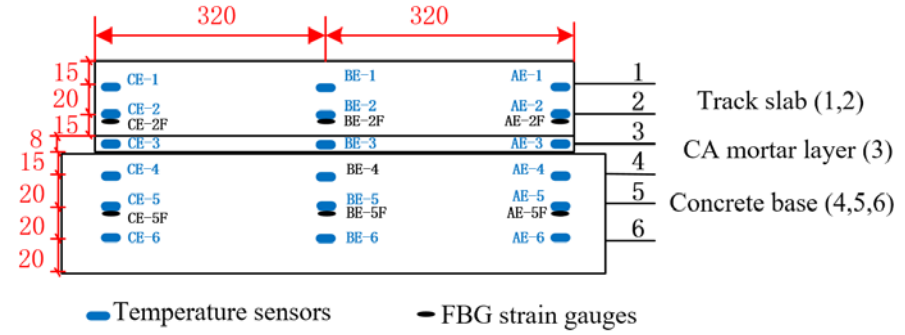

(a) Vertical measurement of section E

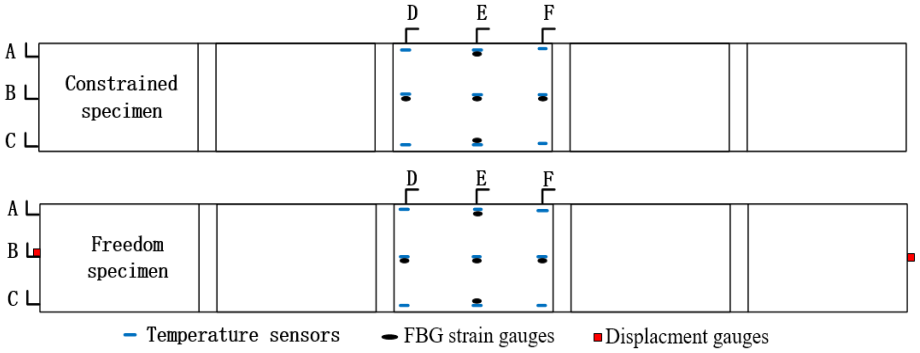

(b) Longitudinal measurement of specimens

Figure (4): Measurement sensors' arrangement

Testing Conditions

Southern China has a typical sub-tropical monsoon climate, with high temperature and humidity in summer. The temperature is usually around 30°C for a long time and the relative humidity is above 80%. Zhong et al. (2018) have defined continuous high temperatures in detail. Therefore, the characteristic temperatures of the test were selected as 26~35°C (12h-35°C to simulate the daytime temperature environment and 12h-26°C to simulate the night temperature environment), while the relative humidity (RH) was 95%, in order to represent the continuous high-temperature and high-humidity environment, as shown in Fig. 5.

EXPERIMENTAL RESULTS

Vertical Temperature Distribution Law

Vertical Temperature Distribution

The highest temperature in the testing chamber can be set at 35°C and the lowest temperature at 26°C. The uniform temperature field of CRTS II slab ballastless track on the bridge in the most unfavorable continuous high-temperature and-humidity environment for a day was simulated. In this paper, the temperature test results corresponding to the most representative cross-section E of the span track slab are used to investigate the temperature distributions of the track structure. The vertical temperature-variation distributions of the two scaled models under different boundary conditions are shown in Fig. 6.

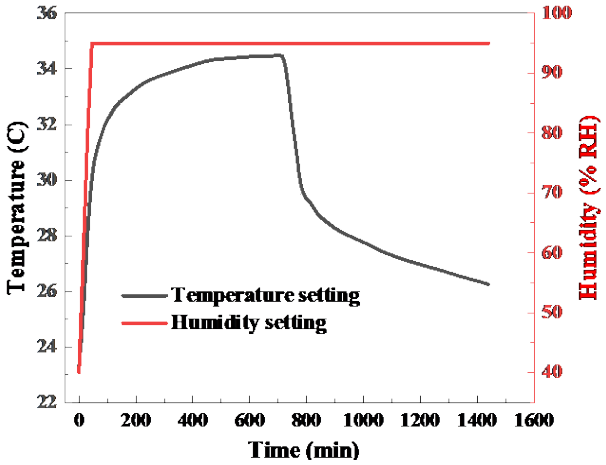

Figure (5): Temperature and humidity input diagram

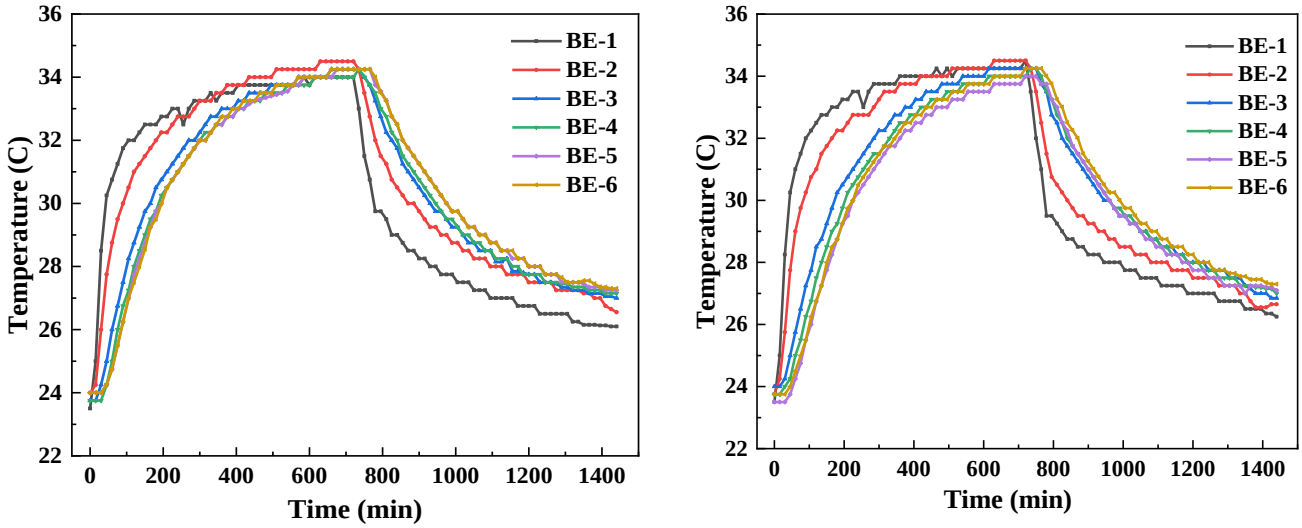

（a）Temperature-time curve of constrained specimen　　（b）Temperature-time curve of free specimen

Figure (6): Temperature-time curves of the test model

It can be seen from Fig. 6 that the temperature of the track structure becomes higher or lower at different locations with the increase or decrease of the environment temperature and the temperature change rate at the top and bottom of the track slab is much larger than at the other locations. The temperature change rate of the top surface BE-1 of the track slab during heating and cooling is the fastest. Taking the CA mortar layer BE-3 as the boundary, the temperature-curve gaps between the bottom surface BE-2 of the track slab, the top surface BE-1 of the track slab and the CA mortar layer BE-3 are larger. Due to the lag effect of temperature transfer between layers, the curve gaps between the CA mortar layer BE-3 and the top surface BE-4 of the concrete base are small. Furthermore, the temperature-time curves of the vertical layers of the test model intersect at different times, resulting in a negative temperature difference.

From the above analysis, the temperature change of each layer of the constrained and free specimens is similar to the changing trend of the ambient temperature, but there are still differences. The temperature–time history curves of the upper and lower track slabs of the constrained specimen intersect at approximately 360 min. However, the temperature–time history curves of the free specimen intersect at approximately 552 min, lagging behind the constrained specimen. Moreover, the temperature curve gap between the upper and lower surfaces of the track slab of the constrained specimen is wider than that of the free specimen during the cooling phase. Nevertheless, the temperature curve gap between the track slab and the CA mortar layer of the constrained specimen is narrower than that of the free specimen.

Three-dimensional Temperature Distribution of Track Structure

The three-dimensional distribution of the transverse and vertical temperature distributions of ballastless tracks with different boundary conditions in a continuous high-temperature and-humidity environment was as shown in Fig. 7. It can be seen from Fig. 7 that the three-dimensional temperature distributions of the constrained specimen and the free specimen show relatively significant non-linear distributions. In the heating stage (40 min, 360 min), the temperature at the middle of the track slab is lower than that at the other parts and the most obvious is the free specimen in the 40^{th} min. In the cooling stage (1080 min, 1335 min), the transverse temperature distribution has a significant influence on the overall temperature distribution of the track structure. Furthermore, under the two boundary conditions, the track structure forms a high-temperature core in the concrete base at the cooling stage. The reason is that the thermal-insulation performance of CA mortar is more obvious than that of ordinary concrete, which has a blocking effect on the temperature conduction inside the structure, while the box girder blocks the heat loss in the middle of the concrete base. Therefore, high-temperature cores are generated in the track slab in the heating stage while the concrete base in the cooling

stage, which complicates and intensifies the effect of the interlayer-temperature gradient of the ballastless track. The blocking effect of the CA mortar layer on temperature transfer is a significant factor affecting the non-linear distribution of the three-dimensional temperature distribution of the ballastless track.

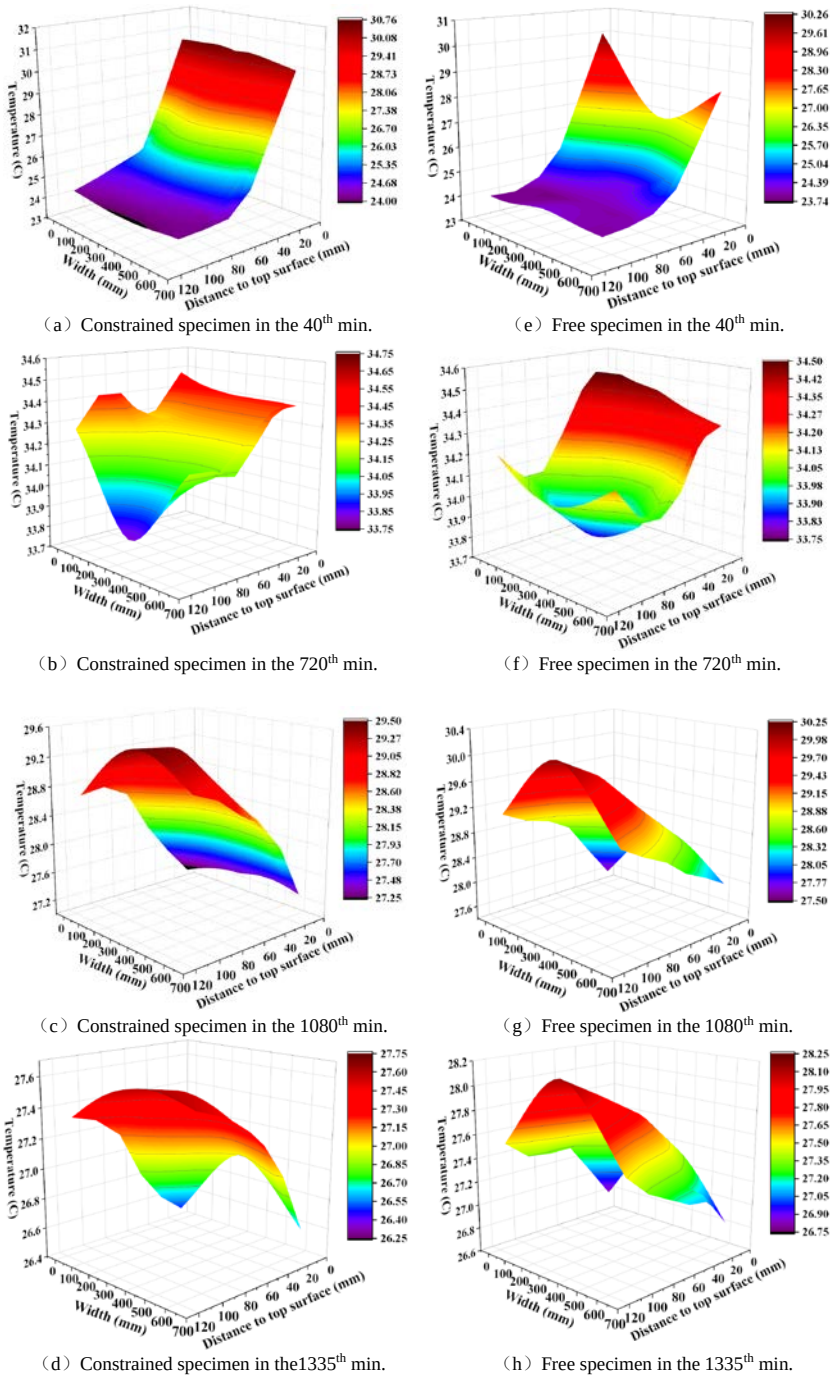

（a）Constrained specimen in the 40th min.
（e）Free specimen in the 40th min.
（b）Constrained specimen in the 720th min.
（f）Free specimen in the 720th min.
（c）Constrained specimen in the 1080th min.
（g）Free specimen in the 1080th min.
（d）Constrained specimen in the1335th min.
（h）Free specimen in the 1335th min.

Figure (7): Transverse and vertical three-dimensional temperature distribution curves of the test specimens

Vertical Temperature Gradient Distribution

To obtain the most unfavourable structural layer of the track structure subject to temperature under different boundary conditions, a comparative analysis of the inter-and intra-storey temperature gradients of the track structure system was carried out, as shown in Fig. 8.

The results indicated that the maximum positive temperature gradient in the constrained specimen is 147 ℃/m, which appears at the interface between the track slab and the CA mortar layer, while the maximum negative temperature gradient is -112.5℃/m, which appears to be in the track slab. In the free specimen, the maximum positive temperature gradient is 171°C/m, while the maximum negative temperature gradient is 105 °C/m, both of which appear at the interface between the track slab and the CA mortar layer. In addition, the negative temperature gradient between the track slab of the constrained specimen and the CA mortar layer is -65.8 °C/m, which is reduced by 37.3% compared with that of the free specimen.

From the above analysis, it can be seen that the vertical temperature gradient of the track slab and the CA mortar layer changes significantly. The most unfavourable positive temperature gradient of the constrained specimen and the free specimen occurred at the interface between the track slab and the CA mortar layer. Therefore, the track slab and the CA mortar layer are greatly affected by the vertical temperature gradient and are prone to experience upwarp deformation, warping deformation, among others, which is the same as the field-survey results. Moreover, the positive and negative temperature gradients between the track slab and the CA mortar layer of the constrained specimen are less than those of the free specimen, indicating that the free boundary of the ballastless track is not conducive to the conduction of temperature between the slab and the CA mortar layer.

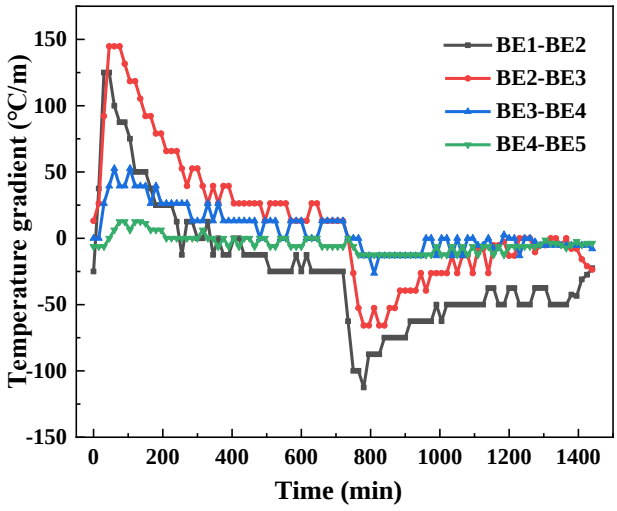

（a）Temperature gradient time-history curve of constrained specimen

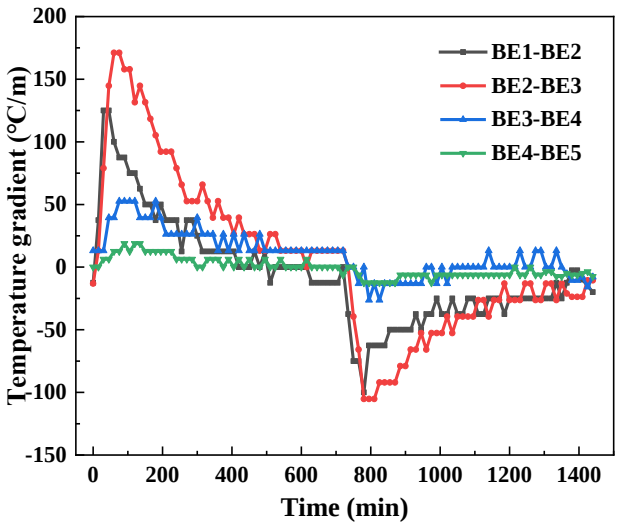

（b）Temperature gradient time-history curve of free specimen

Figure (8): Time-history curves of vertical temperature gradient of the constrained and free specimen

Structural Stress of Ballastless Track

The stress curves of the track structure with different boundary conditions under continuous high-temperature and-humidity environment are shown in Fig. 9. As time increases, the ambient temperature rises from room temperature to 36°C and then cools to 26°C. The longitudinal stresses in the track slab and the concrete base tend to increase and then decrease and the stresses' sequence at different locations is different. Moreover, by comparing and analyzing the stresses at five positions of the track slab with fixed constrained boundary, the maximum compressive stress appears in the left position of CE-2 at the midspan with a value of 4.85 MPa and the maximum tensile stress appears in the middle point of BD-2 at the first end with a value of 1.34 MPa. Different from the track slab, the maximum compressive stress of the concrete base occurs in the middle position of BE-5 at the midspan with a value of 5.8 MPa, while the minimum compressive stress occurs in the right position of AE-5 at the midspan with a value of 0.89 MPa.

As for the free specimen, the maximum compressive stress of the track slab appears in the right position of BD-2 at the midspan with a value of 5.86 MPa, while the maximum tensile stress appears in the middle point of BF-2 at the second end with a value of 1.57 MPa. The maximum compressive stress of the concrete base

appears in the left position CE-5 at the midspan with a value of 5.13 MPa, while the minimum tensile stress appears in the middle position of BE-5 at the midspan with a value of 0.34 MPa. In summary, the stress variation trends of the track slab and the concrete base under different boundary conditions are similar. There are differences in the order of stresses at each point for different boundary conditions, which may be due to the fact that the constraint at both ends perturbs the internal stresses in the track slab, causing a redistribution of stresses in the track structure.

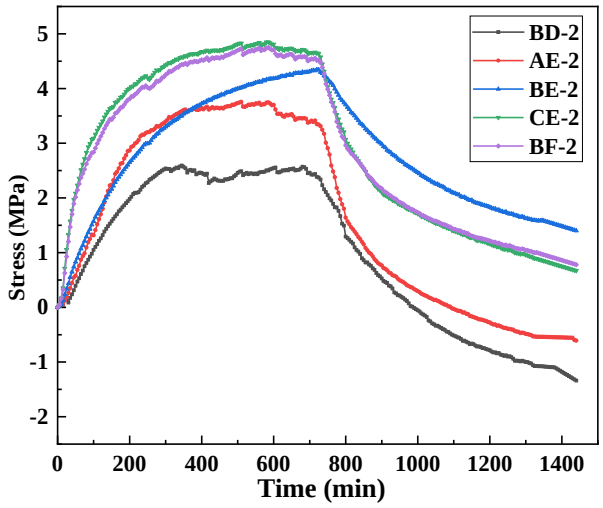

（a）Track slab of constrained specimen

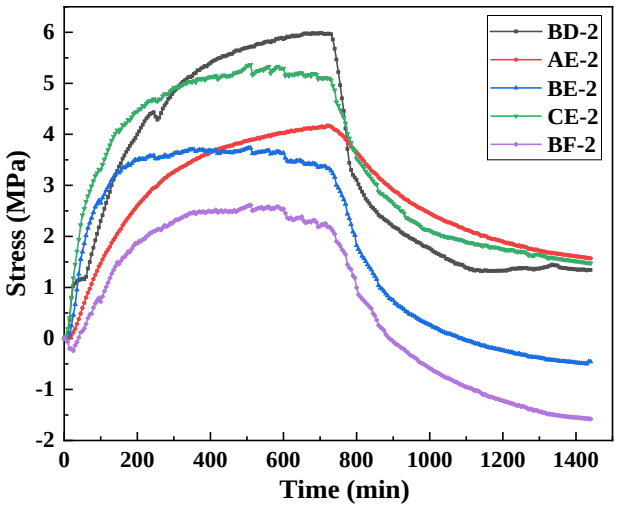

（b）Track slab of free specimen

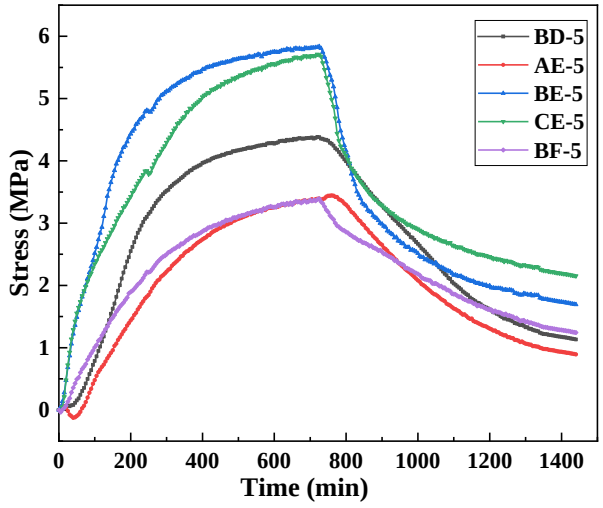

（c）Concrete base of constrained specimen

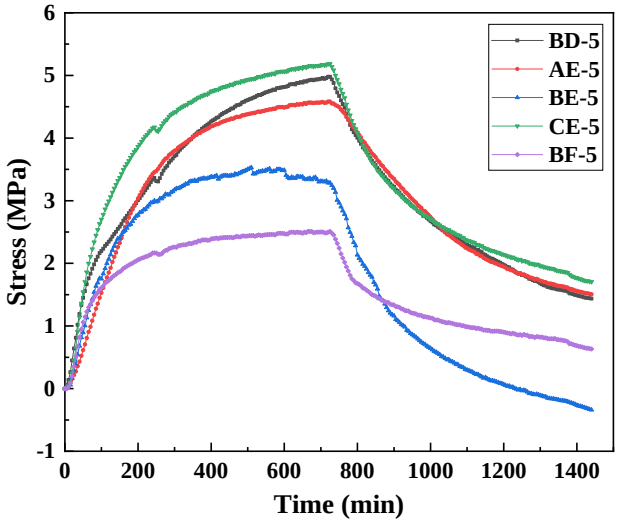

（d）Concrete base of free specimen

Figure (9): Stress curves of the track structure with different boundary conditions

In addition, the relationship between the internal temperature of the track structure and the corresponding longitudinal stress is shown in Fig. 10. The results indicate that the track slab and the concrete base stress and temperature can be fitted with a quadratic polynomial, which is found to be in good agreement in the continuous high-temperature and high-humidity environment. The quadratic polynomial fitting accuracy R^2 is about 0.95, which is a high fitting accuracy, indicating a more reliable regression model. It is indicating that these longitudinal stresses are closely related to the internal temperature.

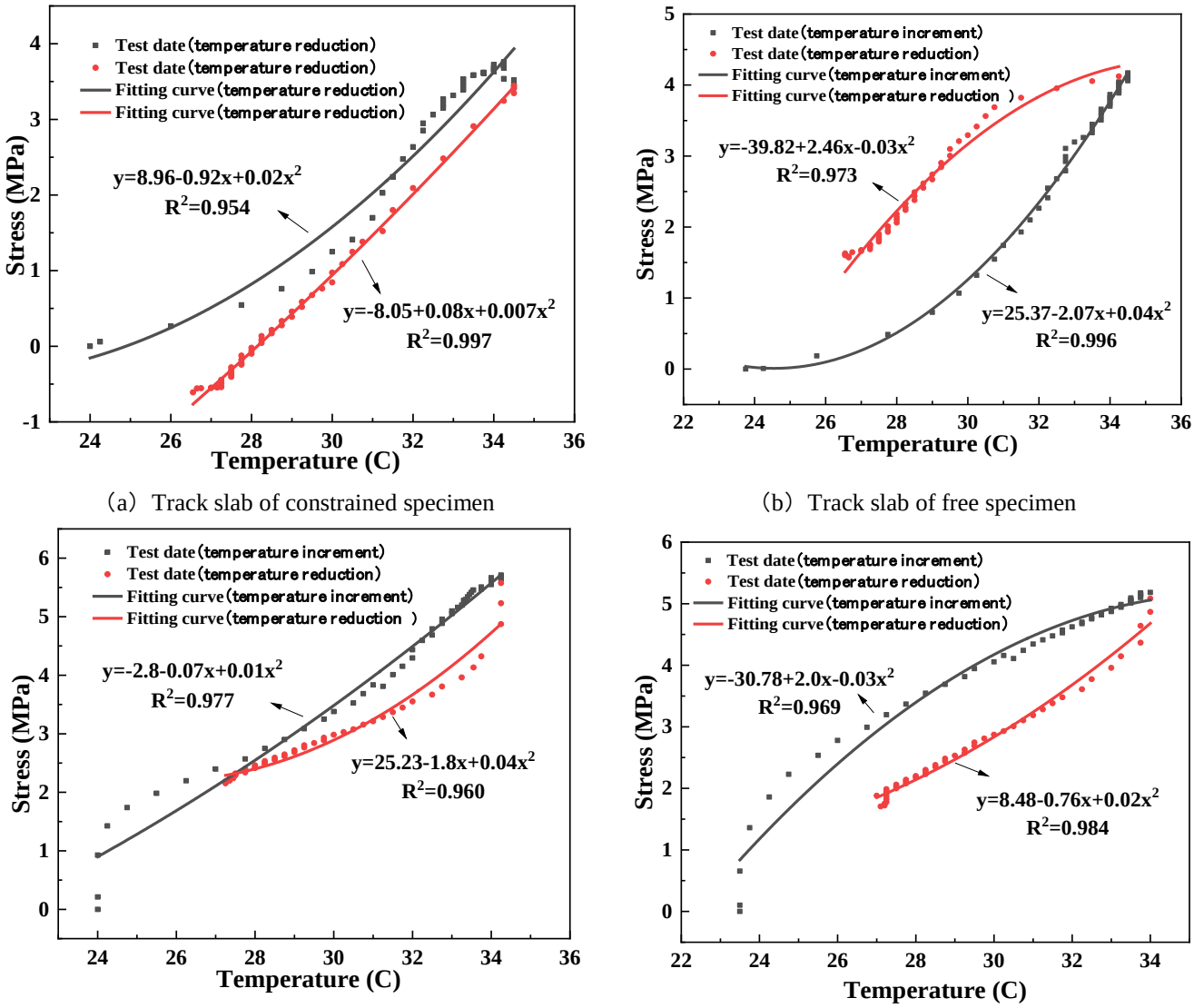

(a) Track slab of constrained specimen

(b) Track slab of free specimen

(c) Concrete base of constrained specimen

(d) Concrete base of free specimen

Figure (10): Temperature-longitudinal stress fitting curves

Track Structure Displacement

In this paper, the longitudinal relative displacement variation law between the track slab and the concrete base of the track structure was investigated. The time-history curves of the relative displacement of the track slab and the concrete base in the free specimen are shown in Fig. 11. As shown in Fig. 11, the relative displacement increases with increasing time. The process can be divided into four stages according to the change rate of the relative displacement: 1) From 0 ~ 260 min, the relative displacement of the track slab and the concrete base increases rapidly. 2) From 260 ~ 694 min, the relative displacement of the track slab and the concrete base increases gently. 3) From 694 ~ 747 min, the relative displacement of the track slab and the concrete base increases briefly. 4) From 747 ~ 1440 min, the relative displacement of the track slab and the concrete base decreases gradually. Moreover, the maximum relative displacement of the track slab and the concrete base is 0.0495 mm, while the minimum longitudinal displacement is 0.012 mm.

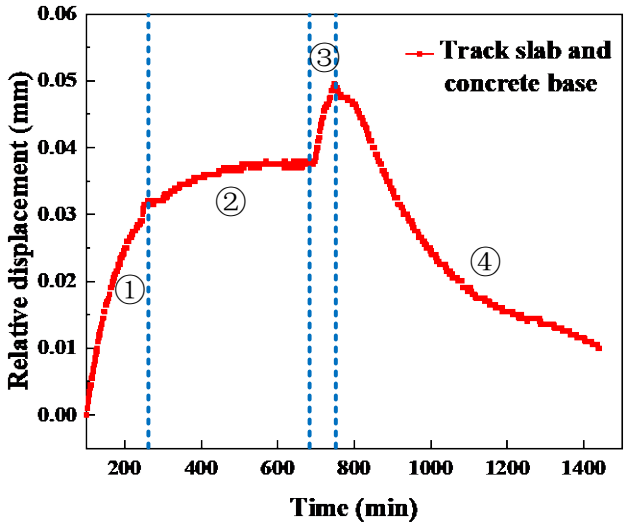

Figure (11): Longitudinal displacement-time curve of the free specimen

The above experimental studies show the pattern of longitudinal displacement of the track structure with time. To investigate the restraining capacity of the CA mortar layer on the track slab, the following theory is introduced. According to the theoretical longitudinal displacement methods for the track slab (Zhou et al., 2022), the theoretical longitudinal displacement of the track slab with a length of 8 m for the free specimen can be calculated by Eq. (1). The longitudinal displacement of the free track slab is illustrated in Fig. 12. The theoretical longitudinal displacements of the track slab for the free specimen are 0.096 mm and 0.024 mm under the maximum environmental temperature of 36℃ and the minimum environmental temperature of 26℃, respectively. Nevertheless, the testing longitudinal displacements of the track slab for the free specimen are 0.067 mm and 0.015 mm under the maximum environmental temperature of 36℃ and the minimum environmental temperature of 26℃, respectively. The testing displacements are smaller than the theoretical displacement responses because of the constraint action of the CA mortar layer on the track slab.

$$\Delta L = L\alpha\Delta T \tag{1}$$

where L is the length of the structure, α is the thermal expansion of concrete, with the value of 1.0 ×10^{-5}/℃. ΔT is the difference between the structure temperature and the ambient temperature.

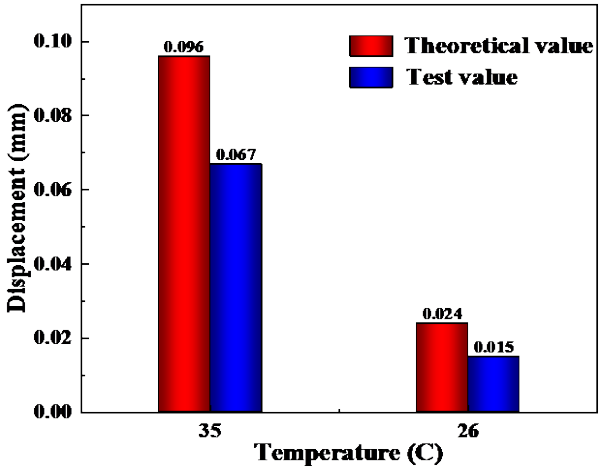

Figure (12): The longitudinal displacement of the free track slab

In short, under the high-temperature and high-humidity environment, the longitudinal displacement of the track slab is significantly affected. The longitudinal displacements of the concrete base and the track slab form a displacement difference, which is easy to create dislocation in the mortar layer, resulting in damage to the mortar layer.

Numerical Analysis of Track Structure

Finite-element Modeling

COMSOL Multiphysics software was used to establish the thermodynamic model of this scaled model under constraint conditions at both ends. The finite-element model was established for the indoor scaled model. The material parameters and dimensions of the

finite-element model are shown in Tables 1 and 2, respectively. The whole structure was assembled and solid elements were used for the track slab, CA mortar layer, concrete base and simply supported box beam. The reinforcement was simplified using beam elements and the model meshes with top-down mapping. There were 44884 domain elements in the whole structure. In order to ensure the grid quality, the main structure and the box girder grid were divided by hexahedron and triangular prism, respectively. The schematic diagram of the model is shown in Fig. 13. To simulate the force characteristics of the track-bridge structure, non-linear spring connections are used between the track slab and the mortar layer, the mortar layer and the base slab and the base slab and the beam to simulate the longitudinal resistance of the structural layers. Spring bases were used at both ends and at the bottom of the structure for the constrained specimen. The coupling of solid mechanics and heat transfer is selected to synchronously solve the thermodynamic response of ballastless track structure under the above-mentioned test environment of high temperature and high humidity.

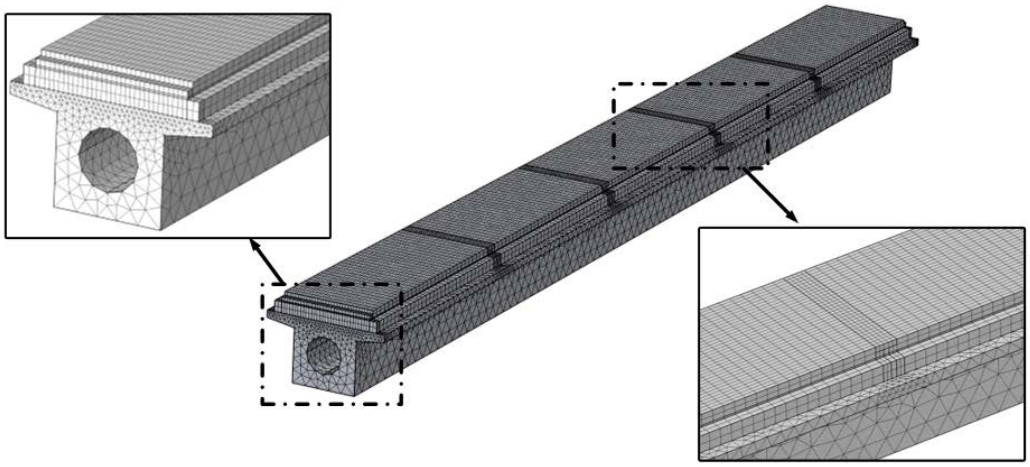

Figure (13): Finite-element model of the track structure

Simulation Model Validation

The correctness of the thermodynamic model was verified through comparing the temperature field obtained by numerical simulation with that of the scale model. When verifying the numerical simulation model, the measured temperature data of the constrained specimen was selected as the temperature load boundary condition to load the track structure. The time curves of temperature variation of the track structure at different depths were obtained by numerical simulation, as shown in Fig. 14.

As shown in Fig. 14, the variation of the numerical simulation results is basically consistent with that of the experimental measurement results and the numerical difference in the temperature-time curves is small. The maximum difference between the two is 2.25°C and the error percentage is 6%. The error is small, which meets the requirements of engineering accuracy.

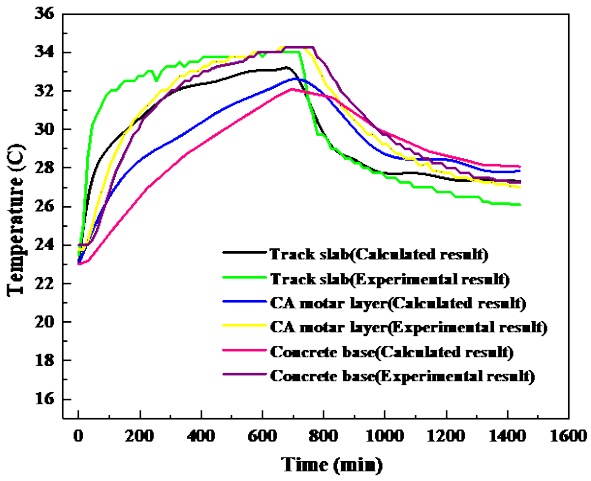

Figure (14): Experimental and calculated test results

Three-dimensional Temperature Field Distribution

The structural temperature distribution of the

constrained specimen is shown in Fig. 15. It can be seen that the upper temperature of the mid-span track slab increases to 33°C and then decreases to 28°C. The temperature change rate of the track slab is the fastest, which is basically consistent with the experimental results.

The temperature field of the constrained specimen at different times is obtained by numerical simulation, as shown in Fig. 15. In Fig. 15(a), in the 12th hour, the maximum temperature point of the three-dimensional temperature field is 34.3°C at the end of the track slab, 33.4°C on both sides of the mid-span track slab and 31.8°C at the middle of the bottom of the concrete base. In Fig. 15(b), in the 24th hour, the maximum temperature point of the three-dimensional temperature field is 28.4°C inside the box girder, the minimum temperature is 26.1°C on the surface of the track slab and the middle temperature at the bottom of the concrete base is 28.2°C. In addition, a high-temperature core is formed inside the concrete base during the cooling phase.

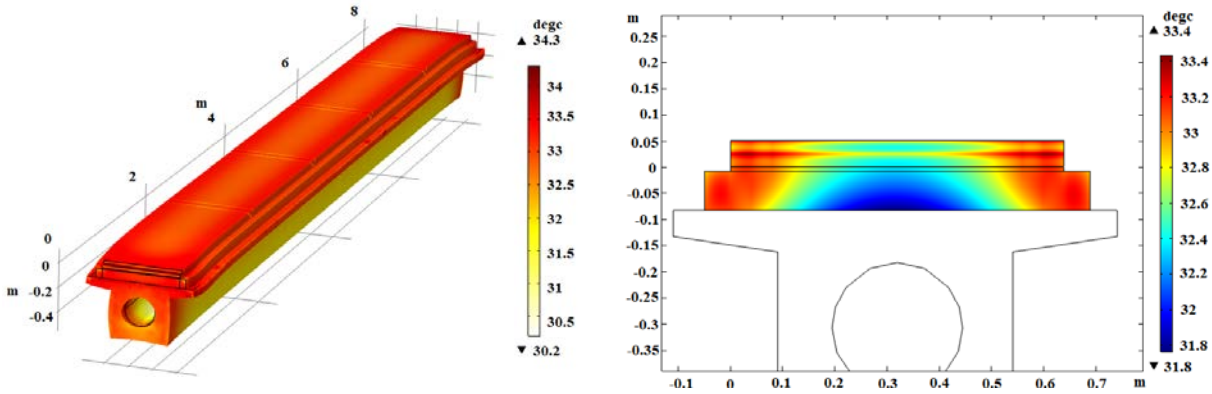

（a）Temperature-field distribution in the 12th hour

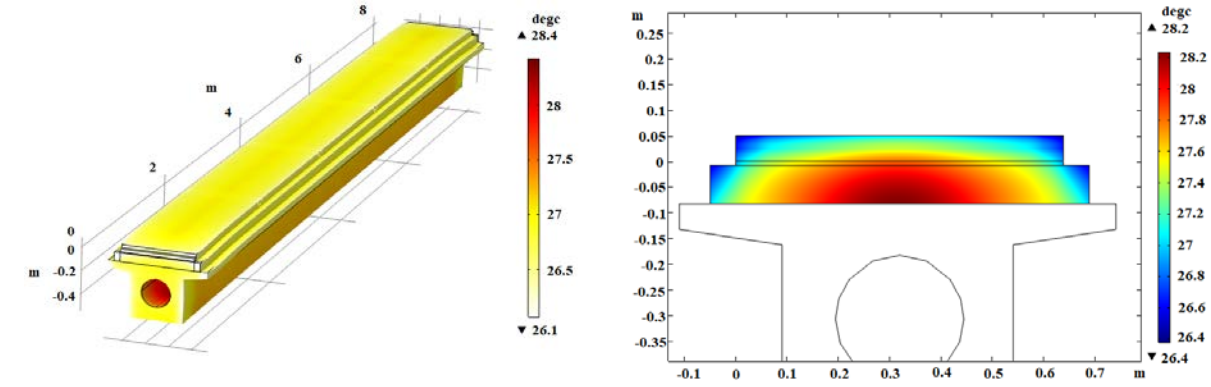

（b）Temperature-field distribution in the 24th hour

Figure (15): Three-dimensional temperature field of constrained specimen

Distribution of Three-dimensional Stress Field

The stress field of the constrained specimen at different times is obtained by numerical simulation, as shown in Fig. 16. From Fig. 16(a), in the 12th hour, the maximum stress point at the end of the track slab is 29.5 MPa and the minimum stress is 0.25 MPa in the box girder. It should be noted that the actual maximum stresses at the ends of the track slab are less than 29.5 MPa, because the numerical model does not remove the local stresses at the ends of the constrained specimen. In addition, the stress is 2.64 MPa on both sides of the track slab at the midspan and the lower part of the concrete base, the stress is 2.16 MPa. From Fig. 16(b), in the 24th hour, the maximum stress point of the three-dimensional stress field is still 13 MPa at both ends of the track slab and the minimum stress is 0.09 MPa in the box girder. The stress at the bottom of the concrete base is 1.3 MPa and the stress at both sides of the track slab is 0.83 MPa.

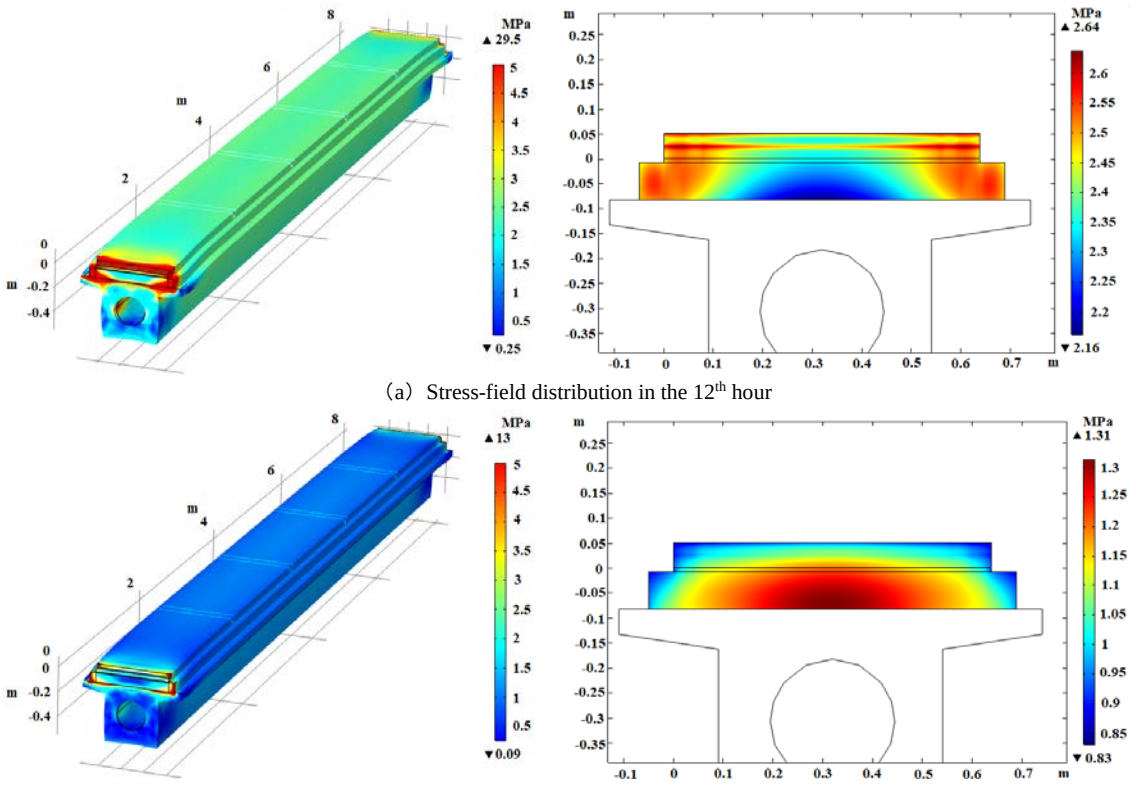

（a）Stress-field distribution in the 12th hour

（b）Stress-field distribution in the 24th hour

Figure (16): Three-dimensional stress field of constrained specimen

CONCLUSIONS

In this study, based on experiments and simulation analysis, the temperature distribution, stress and displacement change laws of the CRTS II slab ballastless track in a humid and hot environment were revealed. The following conclusions can be drawn:

(1) There is a hysteresis phenomenon in the interlayer-temperature transfer and the interface between the track slab and the CA mortar layer is greatly affected by the vertical temperature gradient. The temperature gradient of the track slab-CA mortar layer of the constrained specimen is less than that of the free specimen, indicating that the free boundary of the ballastless track is not conducive to the temperature conduction between the track slab and the CA mortar layer. The three-dimensional temperature distribution of the scale model shows significant non-linearity and high-temperature cores are generated in the track and the concrete base during the heating and cooling phases, respectively.

(2) The stress variation trends of the track slab and the concrete base under two different boundary conditions are similar. Tensile stress easily occurs at both ends of the track slab and the tensile stress of the constrained specimen is greater than that of the free specimen. There is a good fit for the quadratic-regression relationship between internal temperature and structural stress under different ambient temperatures.

(3) In the free specimen, the maximum relative displacement of the track slab and the concrete base is 0.0495 mm, while the minimum longitudinal displacement is 0.012 mm. The displacement responses of the track slab are smaller than those derived from the ideal theoretical displacement due to the restraint action of the CA mortar layer.

(4) The variation of the numerical-simulation results is basically consistent with that of the experimental-measurement results. The three-dimensional temperature field distribution is similar to the stress-field distribution in the high-temperature and high-humidity environment. In the cooling stage, a high temperature core is generated in the middle of the

base plate and the temperature effect is more significant. The reason may be that the CA mortar layer forms an insulating layer and the heat conduction of the base plate is blocked.

Acknowledgments

The work described in this paper is supported by the National Natural Science Foundation of China (Grant Nos. 52178273 and 52278311), the Natural Science Foundation of Chongqing (Grant No. cstc2021jcyj-msxmX1159), the Chongqing Talent Plan Project (Grant No. cstc2022ycjh-bgzxm0124), the Chongqing Project of Joint Training Base Construction for Postgraduates (Grant No. JDLHPYJD2020004) and the State Key Laboratory of Mountain Bridge and Tunnel Engineering (Grant No. SKLBT-ZD2101).

REFERENCES

Černý, R., and Drchalová, J. (2001). "The effects of thermal load and frost cycles on the water transport in two high-performance concretes." Cement & Concrete Research 31 (8), 1129-1140.

Chen, D.P. (2013). "Multi-physical field coupling simulation of hygro-thermal deformation of concrete". Journal of Southeast University, 43 (03), 582-587.

Cho, Y.K., and Kim. S.M. (2019). "Experimental analysis of crack-width movement of continuously reinforced concrete railway tracks". Engineering Structures, 194, 262-273.

Dai, G.L., Su, H.T., and Yan, B. (2015). "Experimental study on the vertical temperature gradient of longitudinally connected slab ballastless track on bridge in autumn". Journal of Hunan University, 42 (03), 94-99.

Dai, G.L., Su, H.T., Liu, W.S., and Yan, B. (2017). "Temperature distribution of longitudinally connected ballastless tracks on bridges in Summer". Journal of Central South University, 48 (04), 1073-1080.

Dai, G.L., Wen, X.H., and Su, H.T. (2015). "Study on horizontal and vertical temperature gradients of ballastless tracks on bridges in cold seasons". Journal of Huazhong University of Science and Technology, 43 (07), 1-5.

Feng, Y.L., Jiang, L.Z., Zhou, W.B., Lai, Z.P., and Chai, X.L. (2019). "An analytical solution to the mapping relationship between bridge structures' vertical deformation and rail deformation of high-speed railways". Steel and Composite Structure, 33 (2), 209-224.

Jiang, L.Z., Feng, Y.L., Zhou, W.B., and He, B.B. (2019). "Vibration characteristic analysis of high-speed railway simply supported beam bridge-track structure system". Steel and Composite Structure, 31 (6), 591-600.

Li, X. (2021). "Durability change of fiber-reinforced concrete under temperature humidity coupled cycle". New Building Material, 48 (07), 82-84.

Lim, N.H., Park, N.H., and Kang, Y.J. (2003). "Stability of continuous welded rail track". Computers & Structures, 81 (09), 2219-2236.

Liu, Y., and Zhao, G.T. (2013). "Analysis of early gap between layers of CRTS Ⅱ slab ballastless track structure". China Railway Science, 34 (04), 1-7.

Liu, Y., Dai, G.L., and Kang, C.J. (2015). "Comprehensive comments on simply-supported girders of high-speed railway in China". Journal of Railway Engineering Society, 12 (02), 242-249.

Min, H.G., Zhang, W.P., Gu, X.L., and Černý, R. (2017). "Coupled heat and moisture transport in damaged concrete under an atmospheric environment". Construction and Building Materials, 143, 607-620.

Qin, G., Huang, P.Y., Zhou, H., Guo, X.Y., and Zheng, X.H. (2016). "Fatigue and durability behavior of RC beams strengthened with CFRP under hot-wet environment". Construction & Building Materials, 111,735-742.

Salama, A., Eraky, A., Yahya, M., and Samir, R. (2022). "Dynamic analysis of high-speed railway bridges applying bridge-vehicle interaction". Jordan Journal of Civil Engineering, 16 (3), 402-416.

Setiawan, D.M (2022). "Sub-grade service life and construction cost of ballasted, asphaltic underlayment and combination rail track design". Jordan Journal of Civil Engineering, 16 (2), 173-192.

Shoukry, S.N., William, G.W., Downie, B., and Riad, M.Y. (2010). "Effect of moisture and temperature on the mechanical properties of concrete". Construction and Building Materials, 25 (2), 688-696.

Wang, J.F., Zhou, Y.B., Wu, T.M., and Wu, X. (2019). "Performance of cement asphalt mortar in ballastless slab track over high-speed railway under extreme climate conditions". International Journal of Geomechanics, 19 (5), 04019037.1-04019037.11.

Wang, S.R., Sun, L., Li, Q.Y., and Wu, Y.S. (2009). "Temperature measurement and temperature-stress analysis of ballastless track slabs". Journal of Railway Engineering Society, (02), 52-55.

Yang, J.J., Zhang, N., Gao, M.M., and Sun, J.L. (2016). "Temperature warping and its impact on train- track dynamic response of CRTS II ballastless track".Engineering Mechanics, 33 (04), 210-217.

Yang, R.S., Li, J.Y., Kang, W.X., Liu, X.Y., and Cao, S.H. (2017). "Temperature characteristics' analysis of the ballastless track under continuous hot weather". Journal of Transportation Engineering - Part A: Systems, 143 (9), 04017048.1-04017048.10.

Zhao, L., Zhou, L.Y., Zhang, G.C., Wei, T.Y., and Zhang, Y.Y. (2020). "Experimental study of the temperature distribution in CRTS Ⅱ ballastless tracks on a high-speed railway bridge". Applied Sciences, 10 (6),1980.

Zhao, L., Zhou, L.Y., Zhang, Y.Y., Yuan, Y.H., Zou, L.F., and Yu, Z.W. (2021). "Experimental study on temperature distribution of CRTS II ballastless track on high-speed railway bridge in summer". Journal of Railway Engineering Society, 18 (02), 287-296.

Zhong, Y., He, Y.L., Lu, H.Y., and Li, Z.W. (2018). "Analysis of interface seam of CRTS II slab track under sustained high temperature". Journal of Railway Engineering Society, 15 (05), 1128-1133.

Zhou, L.Y., Wei, T.Y., Zhang, G.C., Zhang, Y.Y., and Mahunon, A. (2020). "Experimental study of the influence of extremely repeated thermal loading on a ballastless slab track-bridge structure". Applied Sciences, 10 (2), 461.

Zhou, L.Y., Zhang, Y.Y., Yu, Z.W., Zhang, G.C., Zhao, L., and Yuan, Y.H. (2020). "Experimental study on interlaminar displacement of CRTS II ballastless track on bridge under temperature load". Journal of Central South University, 51 (08), 2093-2101.

Zhou, R., Zhu, X., Ren, W.X., Zhou, Z.X., Yao, G.W., Ma, C., and Du, Y.L. (2022). "Thermal evolution of CRTS II slab track under various environmental temperatures: Experimental study". Construction and Building Materials, 325, 126699.